American Mineralogist, Volume 70, pages 223–236, 1985

Equilibria in the system MgO–SiO_2–H_2O: experimental determination of the stability of Mg-anthophyllite

J. V. Chernosky, Jr.

Department of Geological Sciences
University of Maine at Orono, Orono, Maine 04469

H. W. Day

Department of Geology
University of California, Davis, Davis, California 95616

and L. J. Caruso

Department of Earth and Planetary Sciences
Massachusetts Institute of Technology, Cambridge, Massachusetts 02139

Abstract

Existing experimental data among anthophyllite (A), enstatite (E), forsterite (F), quartz (Q), talc (T) and water (W) permit a wide variety of thermodynamically consistent phase diagrams (Day and Halbach, 1979). New experimental reversals have been obtained for the reactions $T + E = A$, $T + F = A + W$ and $A + F = E + W$. Additional experimental data for the reactions $T + F = E + W$ and $T = E + Q + W$ (Chernosky, 1976) and $T = A + Q + W$ and $A = E + Q + W$ (Chernosky and Autio, 1979) have resulted in narrower brackets for these reactions. A phase diagram incorporating the seven equilibria of interest with the [Q] invariant point located at 7.7 ± 0.5 kbar, 682 ± 10°C and the [F] invariant point located at 10.5 ± 1.0 kbar, 795 ± 10°C, supports the topology first suggested by Greenwood (1963). This diagram is consistent with all of our experimental data, the molar volumes and heat capacities of the minerals as well as with most published experimental data for the reactions of interest. No other phase diagram topology is permitted by these data. Although the equilibria are well-established in the 0.5 to 6.0 kbar range, the experimental brackets are too wide to permit the unambiguous location of the [Q] and [F] invariant points at low pressure. These reoccur at less than 0.1 kbar and less than 400°C and may be metastable with respect to serpentine-bearing equilibria.

Introduction

Although the system MgO–SiO_2–H_2O was the first to be studied hydrothermally (Bowen and Tuttle, 1949), investigators are still debating details of the phase relations in this system especially as they relate to the Mg-amphibole anthophyllite. Greenwood (1971), Chernosky (1976), Delany and Helgeson (1978) and Day and Halbach (1979) favor phase diagrams in which the higher pressure [Q] and [F] pair of invariant points (schematically illustrated on Fig. 1) is stable whereas Hemley et al. (1977), Chernosky and Autio (1979) and Usdansky et al. (1978) favor phase diagrams in which the low pressure pair of invariant points is stable. Evans (1977) and Day and Halbach (1979) suggested that both pairs of invariant points may be stable.

With the exception of the unreversed experiments of Bowen and Tuttle (1949), experimental data for the equilibria of interest obtained by Fyfe (1962), Greenwood (1963), Skippen (1971), Chernosky (1976), Hemley et al. (1977) and Chernosky and Autio (1979) are in remarkably good agreement and lend confidence in the experimental results. The principal cause of controversy regarding the anthophyllite phase diagram is the lack of sufficiently accurate thermodynamic data with which to extrapolate phase boundaries to *P–T* conditions outside the range in which the experiments were performed. Consider the minerals talc, anthophyllite and orthoenstatite. Although chemically simple, there is a discrepancy of 12.61 kJ in the enthalpy of formation of talc from the elements in the two most comprehensive compilations of thermodynamic data for geologists (Robie et al., 1978 and Helgeson et al., 1978); until recently, calorimetric measurements for orthoenstatite were nonexistent and the only calorimetric data available for anthophyllite were heat of solution measurements (Weeks, 1956).

The purpose of the present communication is to report new experimental equilibrium data for the reactions $T + E = A$, $T + F = A + W$, and $A + F = E + W$ and to present additional experimental data for the reactions $T + F = E + W$, $T = E + Q + W$, $T = A + Q + W$ and

0003–004X/85/0304–0223$02.00

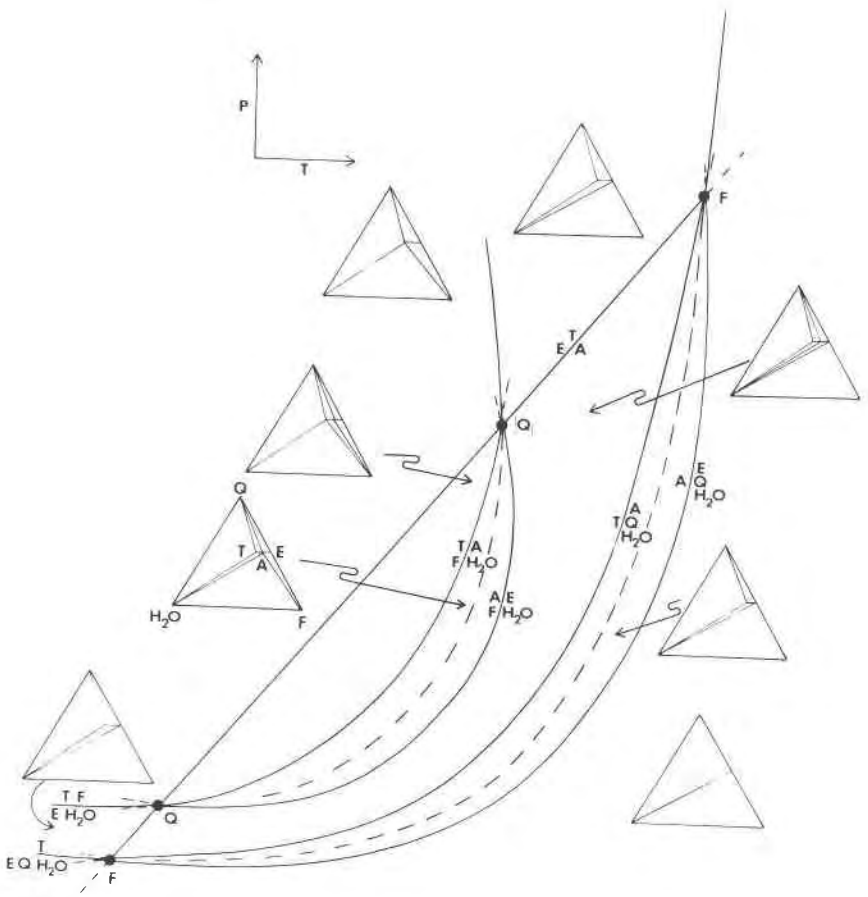

Fig. 1. Schematic phase diagram for anthophyllite after Greenwood (1971) showing the high- and low-pressure intersections of the vapor conservative reaction T + 4E = A with the [Q] and [F] invariant points.

A = E + Q + W. Ours are the first reported reversals for the reaction T + E = A. The pressure–temperature coordinates of all the reactions, with the exception of T + E = A, are well established in the 500–6000 bar range. When combined with the results of Chernosky (1976) and Chernosky and Autio (1979), the new experimental data further constrain the thermodynamic parameters of the minerals of interest. As pointed out by Zen (1977) and emphasized by Helgeson et al. (1978), phase equilibrium data may be used to calculate thermodynamic parameters having an accuracy as good as and in many cases better than that obtainable with calorimetric measurements.

The phase equilibrium data for the seven equilibria listed in Table 1 support the topology of the anthophyllite phase diagram schematically illustrated in Figure 1. Unfortunately, the brackets are still too wide to assign unambiguous P–T coordinates to the low-pressure pair of invariant points. Because the low pressure pair of invariant points occur at water pressures below 100 bars and temperatures below 400°C, they may be metastable with respect to serpentine-bearing assemblages.

The degree to which thermodynamic properties of the solid phases affect the positions of the equilibrium curves drawn through the experimental brackets presented in this paper will be discussed in a companion paper (Day et al., 1985). The data upon which this paper is based were summarized by Chernosky et al. (1982).

Experimental methods

The experimental data recorded in Table 1 were gathered over a period of nine years in four laboratories. During this time, techniques for calibration of hydrothermal equipment, for recording and measuring X-ray powder diffraction patterns, and for determining reaction direction have been modified and refined. Hence, the data are not of equal quality. Nevertheless, our phase equilibrium data are internally consistent and are in reasonable agreement with the data of Greenwood (1963), Skippen (1971), Chernosky (1976), Hemley et al. (1977) and Chernosky and Autio (1979).

Square brackets [ ] are used to name invariant points throughout the paper. The starting material used for reversing a reaction is identified by listing the abbreviations (Table 2) for all solid phases which participate in the reaction. An experiment is identified by listing the abbreviations for all solid phases which participate in the reaction, followed by the number of the experiment. A

Table 1. Experiments bracketing some reactions in the system $MgO–SiO_2–H_2O$

Experiment Number	T (°C)	P_{H_2O} (kbar)	Duration (hours)	Comments	Extent of Reaction
			$T = 3E + Q + H_2O$		
5	691(2)	0.133	220	T(-)E(+)Q(+)	W
40	648(3)	0.5	4896	T(+)E(-)Q(-)A(+)	M
59*R	656(3)	0.5	2160	T(+)E(-)Q(-)	S
35 B	672(2)	0.5	672	T(-)E(+)Q(+)	W
37	681(1)	0.5	1968	T(-)E(+)Q(+)A(+)	S
4	783(2)	0.533	143	T(-)E(+)Q(+)	S
14 R	646(2)	0.598	336	T(+)E(-)Q(-)	S
1 R	717(2)	0.666	740	T(-)E(+)Q(+)	S
7 R	684(2)	0.867	796	T(+)E(-)Q(-)	M
13	660(1)	0.979	144	T(+)E(-)Q(-)	S
32	680(3)	1.0	618	T(+)E(-)Q(-)A(+)	S
58*B	700(6)	1.0	2256	T(+)E(-)Q(-)	S
12 R	721(5)	1.0	623	T(-)E(+)Q(+)	S
9 R	718(2)	1.2	526	T(-)E(+)Q(+)	S
15	635(1)	1.42	166	T(+)E(-)Q(-)	S
3	766(1)	1.466	144	T(-)E(+)Q(+)	S
10	695(3)	1.669	166	T(+)E(-)Q(-)	S
30	729(2)	1.8	2136	T(+)E(-)Q(-)A(+)	M
6 R	717(3)	1.8	552	T(+)E(-)Q(-)	S
2	675(5)	1.866	215	T(+)E(-)Q(-)	S
11	679(5)	1.925	200	T(+)E(-)Q(-)	M
41	744(5)	2.0	1080	T(-)E(+)Q(+)A(+)	S
39	761(5)	2.0	1080	T(-)E(+)Q(+)A(+)	S
53*	780(5)	10.0	46	T(+)E(-)Q(-)	S
54*B	790(5)	10.0	44	T(+)E(-)Q(-)	S
56*B	800(5)	10.0	110	T(-)E(+)Q(+)	S
50*	800(5)	13.0	67	T(-)E(+)Q(+)	M
51*	785(5)	13.6	47	T(+)E(-)Q(-)	S
52*	795(5)	17.0	38	T(+)E(-)Q(-)	S
			$7T = 3A + 4Q + 4H_2O$		
15	613(3)	0.5	1061	T(+)A(-)Q(-)	M
14	630(3)	0.5	1061	T(+)A(-)Q(-)	M
10 B	647(4)	0.5	2544	T(+)A(-)Q(-)	W
12 R	677(1)	0.5	1052	T(-)A(+)Q(+)	M
8 R	664(1)	1.0	744	T(+)A(-)Q(-)	M
5 B	687(3)	1.0	872	T(-)A(+)Q(+)	M
6	714(3)	1.0	744	T(-)A(+)Q(+)	M
19 R	693(3)	1.5	1826	T(+)A(-)Q(-)	W
9 B	701(3)	1.5	1399	T(-)A(+)Q(+)	M
20 R	706(4)	2.0	2760	T(+)A(-)Q(-)	W
17 R	719(2)	2.0	1014	T(-)A(+)Q(+)	W
7	692(1)	3.0	799	T(+)A(-)Q(-)	S
13	720(4)	3.0	1651	T(+)A(-)Q(-)	S
21 B	727(4)	3.0	2688	T(+)A(-)Q(-)	W
16 B	742(4)	3.0	993	T(-)A(+)Q(+)	W
			$A = 7E + Q + H_2O$		
24	664(2)	0.5	837	A(+)E(-)Q(-)T(+)	M
23 B	687(2)	0.5	2607	A(-)E(+)Q(+)	S
11 R	758(3)	0.5	1080	A(-)E(+)Q(+)	W
22 R	700(2)	1.0	816	A(+)E(-)Q(-)	M
21	720(4)	1.0	936	A(+)E(-)Q(-)T(+)	M
19 R	760(1)	1.0	974	A(-)E(+)Q(+)	S
12	737(2)	1.5	1273	A(+)E(-)Q(-)	W
13 B	752(2)	1.5	1224	A(+)E(-)Q(-)	W
14 R	767(4)	1.5	1105	A(-)E(+)Q(+)	M
6	733(2)	2.0	1080	A(+)E(-)Q(-)	M
9 R	751(2)	2.0	630	A(+)E(-)Q(-)	M
5	765(4)	2.0	744	A(+)E(-)Q(-)T(+)	M
25 R	775(2)	2.0	857	A(-)E(+)Q(+)	M
20 R	755(2)	3.0	818	A(+)E(-)Q(-)	M
31*B	810(5)	10.0	89	A(-)E(+)Q(+)	M
30*	820(5)	10.0	70	A(-)E(+)Q(+)	S
			$T + F = 5E + H_2O$		
17 R	600(5)	0.5	3912	T(+)F(+)E(-)	W
16 B	621(2)	0.5	3910	T(-)F(-)E(+)	W
15	635(5)	0.5	3910	T(-)F(-)E(+)A(+)	S
14	620(5)	1.0	2064	T(+)F(+)E(-)	M
8	637(3)	1.0	3910	T(+)F(+)E(-)	S
35*B	652(3)	1.0	2136	T(+)F(+)E(-)	M
7	657(5)	1.0	1053	T(-)F(-)E(+)A(+)	W

Table 1. (Cont.)

Experiment Number	T (°C)	P_{H_2O} (kbar)	Duration (hours)	Comments	Extent of Reaction
2	603(2)	2.0	188	T(+)F(+)E(-)	S
1 R	640(5)	2.0	142	T(+)F(+)E(-)	S
34b*	650(2)	2.0	2472	T(+)F(+)E(-)A(+)	S
3	677(5)	2.0	1968	T(-)F(-)E(+)A(+)	M
4	689(6)	2.0	1968	T(-)F(-)E(+)A(+)	S
18	662(3)	3.0	2794	T(+)F(+)E(-)A(+)	S
33b*	673(3)	3.0	2472	T(+)F(+)E(-)A(+)	S
12	692(5)	3.0	696	T(-)F(-)E(+)A(+)	M
13	703(3)	3.0	696	T(-)F(-)E(+)A(+)	S
11	686(3)	4.0	762	T(+)F(+)E(-)A(+)	W
32*	691(3)	4.0	1896	T(-)F(-)E(+)A(+)	M
9	706(3)	4.0	762	T(-)F(-)E(+)A(+)	S
10 B	722(3)	4.0	762	T(-)F(-)E(+)	S
30*B	679(2)	6.0	1632	T(+)F(+)E(-)	S
31b*	694(2)	6.0	2472	T(-)F(-)E(+)A(+)	M
			$9T + 4F = 5A + 4H_2O$		
11*B	597(7)	0.5	1608	T(+)F(+)A(-)	M
12*B	632(4)	0.5	1776	T(-)F(-)A(+)	W
20*	667(2)	0.5	1728	T(-)F(-)A(+)	M
7*	678(4)	0.5	2184	T(-)F(-)A(+)	M
22*B	626(5)	1.0	3216	T(+)F(+)A(-)	S
21*B	646(5)	1.0	6720	T(-)F(-)A(+)	W
23*R	635(6)	2.0	6696	T(+)F(+)A(-)	S
15*B	660(3)	2.0	1680	T(-)F(-)A(+)	W
14*	680(2)	2.0	1704	T(-)F(-)A(+)	M
8*	633(2)	3.0	1728	T(+)F(+)A(-)	M
3*B	666(4)	3.0	4488	T(+)F(+)A(-)	S
19*R	675(5)	3.0	1728	T(-)F(-)A(+)	W
9*	702(3)	3.0	1464	T(-)F(-)A(+)	M
18*B	677(5)	4.0	1632	T(-)F(-)A(+)	W
10*R	666(4)	5.0	1344	T(+)F(+)A(-)	S
17*B	684(3)	5.0	1392	T(-)F(-)A(+)	W
4*	697(7)	5.0	2520	T(-)F(-)A(+)	W
16*R	716(4)	6.0	1512	T(-)F(-)A(+)	S
			$A + F = 9E + H_2O$		
13*	595(7)	0.5	1608	A(+)F(+)E(-)T(+)	M
14*R	632(4)	0.5	1776	A(+)F(+)E(-)	W
15*B	667(2)	0.5	1728	A(-)F(-)E(+)	S
25*	642(2)	1.0	3336	A(+)F(+)E(-)	W
22*B	677(3)	1.0	3312	A(+)F(+)E(-)	W
21*	660(3)	2.0	1656	A(+)F(+)E(-)	W
24*R	677(3)	2.0	6672	A(+)F(+)E(-)	W
23*	653(4)	3.0	5976	A(+)F(+)E(-)T(+)	W
20*	675(2)	3.0	1704	A(+)F(+)E(-)T(+)	W
1*B	695(2)	3.0	3072	A(-)F(-)E(+)	M
4*	734(2)	3.0	3048	A(-)F(-)E(+)	W
17*	654(2)	4.0	1584	A(+)F(+)E(-)T(+)	M
19*R	677(5)	4.0	1632	A(+)F(+)E(-)	W
10*	632(7)	5.0	1608	A(+)F(+)E(-)T(+)	S
12*	666(4)	5.0	1344	A(+)F(+)E(-)T(+)	S
5*	675(3)	5.0	4368	A(+)F(+)E(-)T(+)	W
18*B	684(3)	5.0	1392	A(+)F(+)E(-)	W
6*R	735(1)	5.0	1968	A(-)F(-)E(+)	S
16*	661(2)	6.0	1680	A(+)F(+)E(-)T(+)	S
8*R	701(6)	6.0	3024	A(-)F(-)E(+)	M
			$T + 4E = A$		
21*	610(2)	4.0	1104	T(+)E(-)A(-)F(+)	S
18*	686(2)	5.0	2064	T(-)E(+)A(+)	S
23*	655(2)	6.0	792	T(+)E(-)A(-)F(+)	S
24*	665(3)	6.0	3552	T(+)E(-)A(-)F(+)	S
25*	674(2)	6.0	3552	T(+)E(-)A(-)F(+)	S
19*	689(3)	6.0	2016	T(-)E(+)A(+)	S
17*	770(5)	8.0	149	T(-)E(+)A(+)	M
14*	770(5)	9.0	143	T(-)E(+)A(+)	W
2*B	730(5)	10.0	4	T(+)E(+)A(-)	M
4*B	755(5)	10.2	65	T(+)E(+)A(-)	M
16*	765(5)	10.0	189	T(+)E(+)A(+)	W
5*	770(5)	10.0	92	T(-)E(+)A(+)	W
8*	785(5)	10.0	115	T(-)E(+)A(-)	W
12*	810(5)	10.0	48	T(-)E(+)A(-)Q(+)	S
11*	840(5)	10.2	22	T(-)E(+)A(-)Q(+)	S

Table 1. (Cont.)

Experiment Number	T (°C)	P_{H_2O} (kbar)	Duration (hours)	Comments	Extent of Reaction
6*B	790(5)	14.0	65	T(+)E(+)A(-)	S
7*	810(5)	13.8	92	T(-)E(+)A(-)Q(+)	M
1*R	780(8)	16.7	49	T(+)E(+)A(-)	S
3*	810(5)	16.9	27	T(-)E(+)A(-)Q(+)	S

Growth or diminution of a phase is indicated by a (+) or (-) respectively. All reactions reversed in the presence of excess H_2O. Parenthesized numbers represent two standard deviations in terms of least units cited for the mean temperatures to their immediate left except for high pressure (>8 kbar) experiments in which the uncertainty is estimated. Symbols S, M and W are qualitative estimates of the extent of reaction and represent greater than 80 percent, 80-30 percent, and less than 30 percent reaction, respectively. *identifies previously unpublished experimental data. R identifies experiments that were included in thermodynamic computations but were redundant; B identifies experiments included in thermodynamic computations that were boundary constraints of the feasible solution space (Day et al., 1984, Table 5).

reaction is named by listing the abbreviations for all phases which participate in the reaction with an equality sign separating the low from the high temperature assemblage. For example, the reaction talc = 3 enstatite + quartz + water is abbreviated T = EQW; the starting material used to reverse this reaction is named TEQ and the designation TEQ-5 refers to experiment #5 listed under the reaction T = EQW in Table 1.

Starting material

Mixtures having the bulk compositions $MgO \cdot SiO_2$, $2MgO \cdot SiO_2$ and $3MgO \cdot 4SiO_2$ were prepared by drying, weighing and mixing appropriate proportions of MgO (Fisher, lot 787699) and SiO_2 glass (Corning lump cullet 7940, lot 62221). SiO_2 glass and MgO were fired at 1000°C for two to three hours to drive off absorbed water. Enstatite, forsterite and talc were synthesized hydrothermally using the oxide mixtures as starting materials; anthophyllite was synthesized hydrothermally in a two- or three-stage process using synthetic talc as a starting material. Examination of the synthetic phases with a petrographic microscope and by powder X-ray diffraction revealed them to be entirely crystalline. Enstatite, forsterite and talc contained trace amounts of impurities which will be described in a later section, whereas anthophyllite contained up to 10% by volume of a triple-chain silicate (Chernosky and Autio, 1979).

Starting materials used to bracket the reactions were prepared by mixing reaction proportions of the high and low temperature assemblages and grinding very lightly for 15 to 30 minutes to ensure homogeneity. Starting materials contained various proportions, ranging from 10 to 90 wt. %, of the high temperature assemblage depending on the particular reaction investigated. Charges were prepared by sealing 5 to 10 mg of starting material together with excess distilled, deionized water in 1.25 cm long gold capsules for low pressure (<7 kbar) experiments and in 1.0 cm long platinum capsules for high pressure (>7 kbar) experiments.

Procedure

Experiments conducted at P_{H_2O} less than 7 kbar. Most experiments bracketing the reactions T = EQW and TF = EW were performed at the U.S. Geological Survey and at the Massachusetts Institute of Technology (MIT), respectively. All other low pressure experiments were performed at the University of Maine. Experiments at the U.S. Geological Survey were conducted in 20.3 cm long, horizontally-mounted, cold-seal hydrothermal vessels. Additional details pertaining to experimental procedure were documented by Chernosky (1973 and 1976). Experiments at MIT and the University of Maine were conducted in 30.5 cm long, horizontally-mounted, cold-seal hydrothermal vessels machined from Haynes Alloy #25 (stellite) or Rene 41. Pressures were measured with factory-calibrated, 40.6 cm Heise gauges certified by the manufacturer as accurate to ±0.1% of full scale (0–4000 bars and 0–7000 bars). In order to conserve valve stems and packings, pressures were monitored carefully at the initiation of each experiment to guard against possible pressure leaks and were then monitored on a weekly or biweekly basis. Minor fluctuations in pressure resulting from temperature drift did occur; however, experiments that suffered pressure drops of greater than 50 bars were discarded. Pressures are believed accurate to within ±50 bars of the stated value.

The temperature of each experiment was recorded daily. The "corrected" mean temperatures together with the uncertainties resulting from daily temperature fluctuations, which are reported as ±2 standard deviations about the mean temperature, are listed in Table 1. Because the low pressure experiments were performed over a period of years during which the experimental techniques were modified, it is important to discuss the corrections which were applied to the mean temperatures reported in Table 1.

Corrections to the mean temperature for experiments performed at the USGS (Table 1, experiments TEQ-1 through 38 and TFE-1 through 4) were obtained in the following manner. Each pressure vessel was positioned in the furnace such that the temperature gradient across the experiment was minimized. A sealed SiO_2-glass tube containing dry NaCl was placed in each pressure vessel and used to calibrate the external, sheathed thermocouples at the melting point of NaCl (800.7°C); thermocouple calibrations were not checked after each experiment. It was believed that this

Table 2. Symbols, abbreviations and chemical formulae

Phase	Chemical Formula	Abbreviation
anthophyllite	$Mg_7Si_8O_{22}(OH)_2$	A
antigorite	$Mg_{48}Si_{34}O_{85}(OH)_{62}$	An
enstatite	$MgSiO_3$	E
forsterite	Mg_2SiO_4	F
quartz	SiO_2	Q
talc	$Mg_3Si_4O_{10}(OH)_2$	T
water	H_2O	W

Equilibrium	Abbreviation
$T = 3E + Q + H_2O$	T = EQW
$7T = 3A + 4Q + 4H_2O$	T = AQW
$A = 7E + Q + H_2O$	A = EQW
$T + F = 5E + H_2O$	TF = EW
$9T + 4F = 5A + 4H_2O$	TF = AW
$A + F = 9E + H_2O$	AF = EW
$T + 4E = A$	TE = A
$2An + 73T = 45A + 90H_2O$	AnT = AW
$9An = 146F + 20A + 259H_2O$	An = FAW
$An = 18F + 4T + 27H_2O$	An = FTW
$180F + 259T = 135A + 4An$	FT = A An

procedure would allow one to account for the difference in temperature between the external measuring thermocouple and the gold sample container within the pressure vessel and to insure internally consistent temperatures among experiments performed in different pressure vessels. Unfortunately, subsequent work revealed two difficulties with this procedure. First, the correction factor varies as a function of temperature making it imperative to calibrate thermocouples over a range of temperatures. Second, the correction factor does not remain constant with time.

Every shielded thermocouple used at MIT and at the University of Maine was calibrated after each experiment against a "standard" thermocouple which had been calibrated previously over a wide range of temperatures using a variety of melting point standards. Use of a "standard" thermocouple insures internally consistent temperatures among experiments performed in different pressure vessels. The difference in temperature between the external measuring thermocouple and the gold sample container within the pressure vessel is accounted for by placing the standard thermocouple inside the pressure vessel while calibrating each external thermocouple. Temperature corrections were usually less than 5°C. Measurements made at atmospheric pressure indicate that temperature gradients in the pressure vessels were less than 1°C over a working distance of 3.0 cm. Hence, error resulting from a temperature gradient along the gold sample containers which were 1.25 cm long was assumed negligible.

It is difficult to ascess the accuracy of the mean temperatures reported for experiments conducted at the USGS principally because there is no way to determine the extent to which the correction factor for each thermocouple changed with time. Based on our experience at the University of Maine, it would be reasonable to add ± 3°C to the reported uncertainty due to temperature fluctuation for experiments performed at the USGS. We believe that the principal source of uncertainty in the reported temperatures of experiments performed at MIT and at the University of Maine is due to temperature fluctuation during the experiment.

All capsules were checked for leaks before and after hydrothermal treatment by heating the capsule to 300°C at room pressure for three minutes and checking for weight loss. After each capsule was opened, the experimental products were examined with a petrographic microscope and by X-ray powder diffraction. Synthetic anthophyllite II was examined with high resolution TEM by D. R. Veblen (Chernosky and Autio, 1979). Due to sluggish reaction rates at temperatures and pressures close to the phase boundary, complete reaction was never observed. Determination of reaction direction at a given temperature and pressure was based on a comparison of an X-ray pattern of an experimental product with an X-ray pattern of the starting material. A number of reflections of product as well as reactant phases were compared in order to judge reaction direction. An experiment was considered successful if a 20% change in the intensities of selected X-ray reflections of an experimental product relative to those of the starting material could be observed. Although microscopic observation of the experimental products generally did not reveal textural evidence that could be used as the sole criterion to judge reaction direction, such observations were often useful supplements to the X-ray data.

Unit-cell parameters for synthetic phases used in the starting material were calculated by refining powder patterns obtained with an Enraf-Nonius FR552 Guinier camera or an 11.46 cm Debye-Scherrer camera and Cu$K\alpha$ radiation; CaF_2 (Baker Lot 91548, $a = 5.4620 \pm 0.005$Å) or BaF_2 ($a = 6.1971 \pm 0.0002$Å) standardized against gem diamond ($a = 3.56703$Å, Robie et al. 1967) was used as an internal standard. Least-squares unit-cell refinements were performed using the computer program of Appleman and Evans (1973).

Experiments conducted at P_{H_2O} greater than 7 kbar. High pressure experiments were conducted in the laboratory of R. C. Newton and J. R. Goldsmith at the University of Chicago, using an 0.75 inch, end load piston-cylinder apparatus. All experiments were conducted in the piston-out mode using a low-friction NaCl pressure cell (Johannes, 1978) wrapped in lead foil and lubricated with dry MoS_2. Experiments were conducted following the methods described by Danckwerth and Newton (1978). The cold assembly was first pressurized below the desired pressure and then heated. Thermal expansion of NaCl during heating ensured piston-out conditions for each experiment. Temperatures were monitored with chromel alumel thermocouples; no correction for the effect of pressure on the emf of the thermocouple was made. Considerable experience with the NaCl pressure cell at the University of Chicago indicates that reasonable pressure and temperature uncertainties are ± 300 bars and ± 5°C, respectively (D. M. Jenkins, pers. comm.)

Results

Synthesis and characterization of phases

Anthophyllite [$Mg_7Si_8O_{22}(OH_2)$] was synthesized in either a two- or three-stage process. The two-stage process involved rapid synthesis (~ 1 day) of anthophyllite from a mixture of oxides having the bulk composition of talc under conditions above its stability field ($P_{H_2O} = 1$ kbar, 815°C), followed by long hydrothermal treatment of the synthetic product within its stability field. The first stage resulted in a mixture of anthophyllite, cristobalite, enstatite, talc and fosterite; the second stage resulted in the recrystallization of these phases to anthophyllite with minor talc and quartz. Chernosky and Autio (1979) used the latter as starting material to reverse the reactions A = EQW and T = AQW. The three-stage process involves the addition of sufficient periclase (MgO) to convert the anthophyllite + talc + quartz mixture synthesized in the two-stage process to anthophyllite.

The unit cell parameters of anthophyllites synthesized in both the two- and three-stage processes, anthophyllite II and anthophyllite III, respectively, are given in Table 3. The unit cell parameters reported for anthophyllite II by Chernosky and Autio (1979) ($a = 18.57 \pm 0.04$Å; $b = 17.9 \pm 0.04$Å; $c = 5.25 \pm 0.01$Å and $V = 1748.0 \pm 3.7$Å^3) differ from the values given in Table 3. We believe that the new refinement given in Table 3 is superior for several reasons. The unit cell refinement reported by Chernosky and Autio was based on 16 reflections whereas the new refinement is based on 27 reflections. A single CaF_2 reflection was used to correct the observed positions of anthophyllite reflections in the earlier refinement; considerable experience with the Guinier camera since the earlier refinement indicates that the correction factor varies monotonically with 2θ and that a correction curve rather than a single value is required for higher accuracy—a correction curve was established before proceeding with the new refinement.

Enstatite [$MgSiO_3$] was synthesized hydrothermally at $P_{H_2O} =$ 1 kbar and temperatures ranging from 800 to 815°C in five to fourteen days. The synthetic enstatite crystals are fine-grained (10μ), prismatic, inclusion-free, often twinned and exhibit parallel extinction. The unit cell parameters of enstatites used by Chernosky (1976) and Chernosky and Autio (1979) are compared with the unit cell parameters of enstatite used in this study in Table 3. Although the molar volume of enstatite I is smaller than

Table 3. Unit cell parameters of natural quartz and synthetic anthophyllite, enstatite, forsterite and talc

Phase	a, Å	b, Å	c, Å	β	V, Å^3	S	N
Quartz* I	4.9124(1)	—	5.4052(2)	—	112.960(6)	Si	13
Anthophyllite II	18.632(6)	17.89(15)	5.251(3)	—	1748.92(1.48)	CaF	27
Anthophyllite III	18.634(17)	17.951(16)	5.270(5)	—	1763.13(1.94)	CaF	19
Enstatite I	18.19(3)	8.763(7)	5.18(2)	—	825(3)	BaF	12
Enstatite II	18.236(10)	8.822(3)	5.176(1)	—	832.86(43)	CaF	19
Enstatite III	18.222(3)	8.822(1)	5.174(1)	—	831.85(15)	CaF	44
Forsterite I	4.769(2)	10.210(15)	5.987(8)	—	291.4(4)	—	31
Forsterite III	4.751(1)	10.198(1)	5.979(1)	—	289.76(5)	CaF	42
Talc I	5.27(4)	9.15(2)	18.66(10)	100 27'	885(8)	BaF	9
Talc II	5.291(6)	9.169(7)	18.982(16)	99 4'	909.47(1.28)	CaF	14
Talc III	5.293(5)	9.175(6)	18.984(11)	99 52'	908.41(71)	CaF	14

Figures in parentheses represent the estimated standard deviation in terms of least units cited for the value to their immediate left; the uncertainties were calculated using a unit-cell refinement program and represent precision only. Abbreviations: I = Chernosky (1976); II = Chernosky and Autio (1979); III = this study; S = X-ray standard; N = number of reflections used in the refinement. *Determined by J.S. Huebner and K. Shaw

the molar volume of enstatites II and III, we believe all enstatites are substantially identical for the following reasons. All enstatites were synthesized from the same starting material under similar P–T conditions. The unit cell refinement for enstatite I was based on measurements of a powder pattern recorded with a Debye–Scherrer camera whereas unit cell refinements of enstatites II and III were based on patterns recorded with a Guinier camera. The Debye–Scherrer powder pattern contains fewer lines all of which were considerably broader than corresponding lines on the Guinier patterns. We believe that the unit cell refinements of enstatites II and III are more reliable than the refinement of enstatite I because the resolution obtainable with a Guinier camera is about twice that obtainable with an 11.46 cm Debye–Scherrer camera. Unfortunately, the entire aliquot of enstatite I was used before a Guinier pattern could be obtained.

Forsterite [Mg_2SiO_4] was synthesized hydrothermally at 800–815°C, P_{H_2O} = 0.5–1 kbar in experiments of 5–20 days duration. Crystals are fine grained (9μ) and anhedral with less than 0.5% impurities. The powder patterns and unit cell parameters (Table 3) compare favorably with those published for synthetic forsterite by Fisher and Medaris (1969).

Talc [$Mg_3Si_4O_{10}(OH)_2$] was synthesized hydrothermally at 600°C, P_{H_2O} = 2 kbar in five to twenty days. The product typically crystallized as aggregates of fine-grained (12μ) plates with relatively low birefringence and contained trace amounts of forsterite as an impurity which may result from saturation of the fluid phase with silica from the starting material or from a starting material deficient in SiO_2. Unit cell parameters for synthetic talc are given in Table 3. Despite the smaller molar volume of talc I compared with talc II and III, we believe that all three talcs are identical. The discrepancy in talc unit cell parameters is probably the result of differences in recording and measuring the powder patterns. The powder pattern for talc I was recorded with a Debye-Scherrer camera and consisted of relatively few, rather broad reflections compared with patterns of talc II and III which were recorded with a Guinier camera. Unfortunately, the supply of talc I was used before its unit cell parameters could be checked. The powder patterns and unit-cell parameters of talc II and III (Table 3) compare favorably with those of natural (PDF 13-558) and synthetic (Forbes, 1971) talc.

Natural quartz [SiO_2] from Minas Gerais, Brazil was added to the starting material used to bracket the reaction T = EQW. The Brazilian quartz, whose unit cell parameters are given in Table 3, was obtained from J. S. Huebner. Synthetic quartz, obtained as a by-product in the two-stage process used to synthesize anthophyllite, was present in the starting material used to bracket the reactions A = EQW and T = AQW. Although the positions of major reflections from the synthetic quartz compare favorably with those of natural quartz from Lake Toxaway, North Carolina (PDF 5-0490), a unit cell refinement was not obtained due to insufficient reflections present on a powder pattern of the starting material.

Experimental data

Experimental data for seven reactions among the phases anthophyllite, forsterite, orthoenstatite, talc, quartz and water are presented in this section. Figure 1 (after Greenwood, 1971) is a schematic phase diagram showing all of the stable equilibria and compatibility relations among the phases of interest; compatibility relations are omitted from subsequent figures for clarity. Two possible locations for each of the two invariant points [Q] and [F] are shown in Figure 1. Experimental data for each reaction are shown on separate P–T diagrams because several of the reactions are so closely spaced that experiments often overlap. Figure 1 provides a convenient frame of reference which allows us to interpret the growth of extraneous phases in many of the experiments.

Before discussing experimental data for each of the reactions, several important features depicted on Figure 1 need to be reviewed: (1) the degenerate reaction TE = A is only stable along the solid line between the invariant points labeled [F], (2) the reactions T = EQW and TF = EW are only stable on the low temperature side of the reaction TE = A, (3) anthophyllite is stable in the region bounded by the stable segments of the reactions TE = A and A = EQW, (4) the assemblage anthophyllite + H_2O is stable throughout all but a portion of the anthophyllite stability field, being unstable in the region bounded by the reactions TE = A and TF = AW. Chernosky (1976), Day and Halbach (1979) and Delany and Helgeson (1978) suggest that the high pressure [Q] and [F] invariant points are stable (upper half of Fig. 1) whereas Hemley et al. (1977), Usdansky et al. (1978) and Chernosky and Autio (1979) suggest that the low pressure [Q] and [F] invariant points (lower half of Fig. 1) are stable. Evans (1977) and Day and Halbach (1979) suggest that both the high and low pressure portions of the phase diagram (Fig. 1) may exist.

Agreement among the low pressure studies of Fyfe (1962), Greenwood (1963), Skippen (1971), Chernosky (1976), Hemley et al. (1977) and Chernosky and Autio (1979) is generally quite good. Although Greenwood used both synthetic phases and natural minerals as starting materials, only those experiments conducted using synthetic phases are plotted on the figures. All of the phase equilibrium data obtained by Chernosky (1976) and by Chernosky and Autio (1979) are included in Table 1 and in the accompanying figures for completeness. Errors resulting from temperature fluctuation for experiments bracketing the reactions T = EQW and TF = EW are not cited by Chernosky (1976) but are included in Table 1. Moreover, additional experiments were conducted in order to improve

the brackets for several reactions; the new experiments are identified by asterisks in Table 1.

Experimental data for the three dehydration reactions emanating from the [F] invariant point will be considered before describing experimental data for the three dehydration reactions emanating from [Q]. The solid–solid reaction TE = A will be considered last because it serves to link the two pairs of [Q] and [F] invariant points. Because several of the reactions occur within a small region of P–T space, product assemblages for five of the equilibria listed in Table 1 often contain phases not present in the starting material. The growth of extraneous phases was minor and did not impair our ability to judge reaction direction. Nucleation and growth of extraneous phases indicates the operation of at least one competing reaction. Unfortunately, it was usually difficult to identify the competing reaction(s). All of the experimental data, including information on the growth of extraneous phases, yields a consistent picture and affords a reasonable interpretation of anthophyllite phase relations. A phase diagram consistent with experimental data recorded in Table 1 is presented in a subsequent section.

The equilibrium curves drawn on Figures 2 through 9 were calculated using the midpoint of the feasible solution space which was obtained by linear programming analysis described by Day et. al. (1985). Experiments in which extraneous phases were present (Table 1) were not included in the calculations. In addition, the errors for each experiment were assumed to be at least ± 5°C, whereas only the error resulting from temperature drift is included in Table 1 and on the figures. The conservative treatment of the data results in calculated equilibrium curves which narrowly "miss" three of the equilibrium brackets (see Figs. 4, 5 and 7). In each case the apparent discrepancy is due solely to the larger possible error in temperature that was assumed in the calculations.

The reaction $T = 3E + Q + H_2O$. Critical experiments bracketing the dehydration curve for the reaction T = EQW are listed in Table 1 and plotted on Figure 2. In addition to the data reported by Chernosky (1976), Table 1 contains eight new experiments six of which were conducted at $P_{H_2O} = 10$ kbar and above. Two different starting materials were used to locate the curve. For experiments conducted at $P_{H_2O} = 2$ kbar and below, the starting material consisted of the reaction proportions of T, E and Q. Anthophyllite spontaneously nucleated and grew (Table 1) in most of the longer experiments suggesting that the reaction TEQ is metastable with respect to anthophyllite-bearing reactions at low pressures. It should be emphasized that anthophyllite growth in all but one experiment (TEQ-30 was minor and in no cases did anthophyllite growth make judging reaction direction ambiguous.

In contrast, several early experiments conducted above $P_{H_2O} = 12$ kbar using the TEA starting material resulted in the decomposition of anthophyllite and the growth of either T or E + Q suggesting that the reaction T = EQW is stable with respect to the anthophyllite-bearing reactions T = AQW and A = EQW at pressures above 12 kbar. In

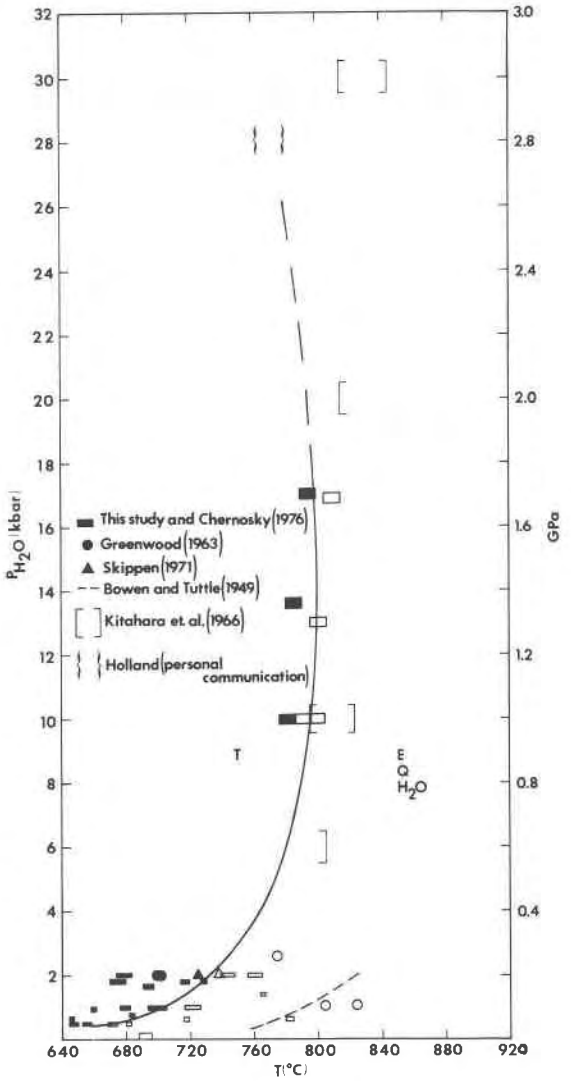

Fig. 2. Dehydration curve for the reaction T = 3E + Q + H_2O. Solid symbols represent growth of talc; open symbols represent growth of the high temperature assemblage. Size of rectangles represents uncertainty in the measurement of pressure and temperature. The curve was not calculated at water pressures above 10 kbar.

subsequent experiments at water pressures above 10 kbar, the TEQ starting material was used to define the position of the reaction T = EQW in P_{H_2O}–T space (Table 1).

Agreement among the low pressure experimental data in Table 1 and the data obtained by Greenwood (1963) and Skippen (1971) for the reaction T = EQW is excellent (Fig. 2). The curve obtained by Bowen and Tuttle (1949) lies about 80°C above the curve obtained in this study (Fig. 2) because these investigators performed synthesis rather than reserval-type experiments.

Tight brackets for T = EQW, were obtained in the pres-

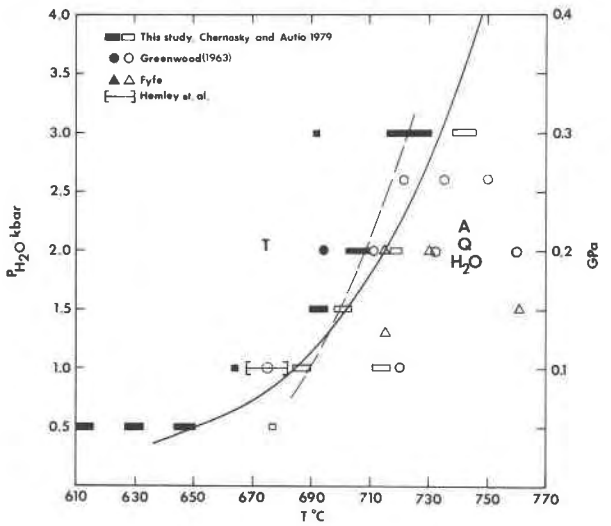

Fig. 3. Dehydration curve for the reaction $7T = 3A + 4Q + H_2O$. Solid symbols represent growth of talc; open symbols represent growth of the high temperature assemblage. Size of rectangles represents uncertainty in the measurement of pressure and temperature. Dashed curve shows where Greenwood (1963) located this equilibrium.

sure range from 10 to 17 kbar (Fig. 2). Extrapolation of the curve to water pressures above 18 kbar, however, necessitates choosing either Holland's (personal communication, 1978 and 1983) preliminary bracket at 28 kbar or the experimental data of Kitahara et al. (1966). The discrepancy between these two data sets amounts to about 50°C at $P_{H_2O} = 25$ kbar. We have opted for Holland's bracket at 28 kbar because his work is more recent and conducted in R. C. Newton's laboratory at the University of Chicago using the same equipment and experimental procedures as those used during this study.

The reaction $7T = 3A + 4Q + 4H_2O$. Critical experiments bracketing the dehydration curve for the reaction T = AQW were performed by Chernosky and Autio (1979); their data are summarized in Table 1 and plotted on Figure 3. Experimental data for the reaction T = AQW obtained by Fyfe (1962), Greenwood (1963), Hemley et al. (1977), Chernosky (1976) and Chernosky and Autio (1979) are remarkably consistent (Fig. 3).

Anthophyllite spontaneously nucleated and grew in a number of long term TEQ experiments. Unfortunately, anthophyllite growth in these experiments does not constrain the position of T = AQW because anthophyllite is stable on *both* sides of this reaction (Fig. 1).

The reaction $A = 7E + Q + H_2O$. Critical experiments bracketing the dehydration curve for the reaction A = EQW are listed in Table 1 and plotted on Figure 4. Table 1 contains four additional experiments which supplement the data reported by Chernosky and Autio (1977) and further constrain the location of the curve. Although two of the experiments, (TEQ-37 and TEQ-39), were performed to bracket the reaction T = EQW (Chernosky, 1976), they may also constrain the location of A = EQW. Anthophyllite spontaneously nucleated and grew in each of these experiments suggesting that it is a stable phase under the conditions of the experiments. Because A = EQW delimits the high temperature side of anthophyllite's stability field, the phase boundary for this reaction probably lies on the high temperature side of experiments TEQ-37 and TEQ-39. Experiment TEQ-37 narrows the bracket at $P_{H_2O} = 500$ bars by 18°C. Although experiment TEQ-39 does not narrow the bracket at $P_{H_2O} = 2000$ bars and hence is not plotted on Figure 4, it does confirm Chernosky and Autio's result at this pressure. Two new experiments at $P_{H_2O} = 10$ kbar, AEQ-30 and AEQ-31, constrain the curve to lie at temperatures below 810°C at this pressure.

Experimental data recorded in Table 1 for the reaction A = EQW are consistent with the experimental data of Fyfe (1962) and Greenwood (1963) and with the equilibrium temperature of 729°C at $P_{H_2O} = 1000$ bars calculated by Hemley et al. (1977). However, the curve obtained in this study has a flatter slope (Fig. 4) than the curve obtained by Greenwood (1963) chiefly due to added constraints imposed by the 500 bar experiments.

The reaction $T + F = 5E + H_2O$. Critical experiments bracketing the dehydration curve for the reaction TF = EW are listed in Table 1 and plotted on Figure 5. In

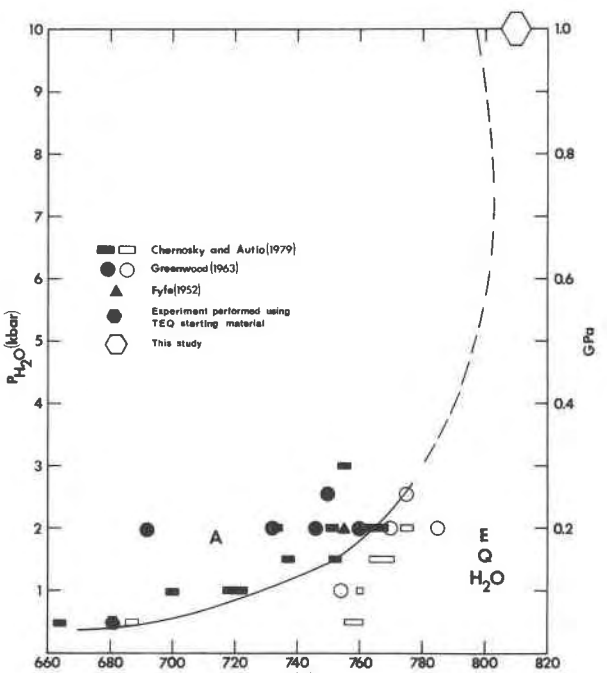

Fig. 4. Dehydration curve for the reaction $A = 7E + Q + H_2O$. Solid symbols represent growth of anthophyllite; open symbols represent growth of the high temperature assemblage. Size of rectangles represents uncertainty in the measurement of pressure and temperature.

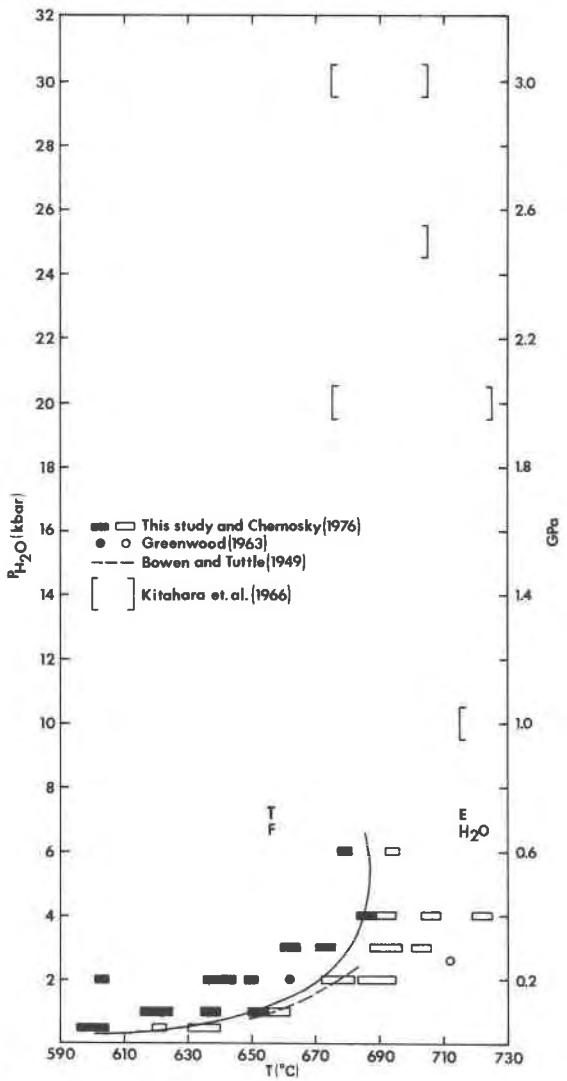

Fig. 5. Dehydration curve for the reaction T + F = 5E + H_2O. Solid symbols represent growth of the low temperature assemblage; open symbols represent growth of the high temperature assemblage. Size of rectangles represents uncertainty in the measurement of pressure and temperature.

addition to the experimental data reported by Chernosky (1976), Table 1 contains seven new experiments conducted with the TFE starting material. The experiments at P_{H_2O} = 6 kbar (Table 1, TFE-30 and -31b) are particularly important because they clearly indicate that the P–T slope of the dehydration curve changes sign at a fairly low pressure. Chernosky (1976, Table 3, experiment #6) reported that the high temperature assemblage grew at 663 ± 3°C, 2 kbar. This experiment was omitted from Table 1 because three more recent experiments (TFE-11, -33b and -35) suggest that the reaction lies at a slightly higher temperature.

Anthophyllite spontaneously nucleated and grew (Table 1) on both the high and low temperature sides of the reaction TF = EW in most of the longer experiments conducted using the TFE starting material. Anthophyllite growth suggests that the reaction TF = EW is metastable with respect to the anthophyllite-bearing reactions TF = AW, AF = EW and/or TE = A under the conditions of the experiments. Anthophyllite growth was minor in all cases and did not interfere with our ability to judge reaction direction.

The experimental data recorded in Table 1 are consistent with Greenwood's (1963) two widely-spaced reversals and indicate that the equilibrium curve lies on the low temperature side of the unreversed curve obtained by Bowen and Tuttle (1949). The high temperature reversal at P_{H_2O} = 6 kbar, 694°C (Table 1) indicates that the high pressure reversals of Kitahara et al. (1966) lie at too high a temperature. This discrepancy probably results from inaccurate calibration of the piston-cylinder apparatus used by these investigators.

The reaction $9T + 4F = 5A + 4H_2O$. Critical experiments bracketing the dehydration curve for the reaction TF = AW are listed in Table 1 and plotted on Figure 6. In addition to the experiments listed under TF = AW, four experiments listed under TE = A (TEA-23, -24, -25 and -19) and plotted as hexagons on Figure 6 and seven experiments listed under AF = EW (AFE-5, -12, -13, -16, -17, -20 and -23) and plotted as solid triangles on Figure 6 are consistent with the location of the curve.

Forsterite nucleated and grew together with talc whereas

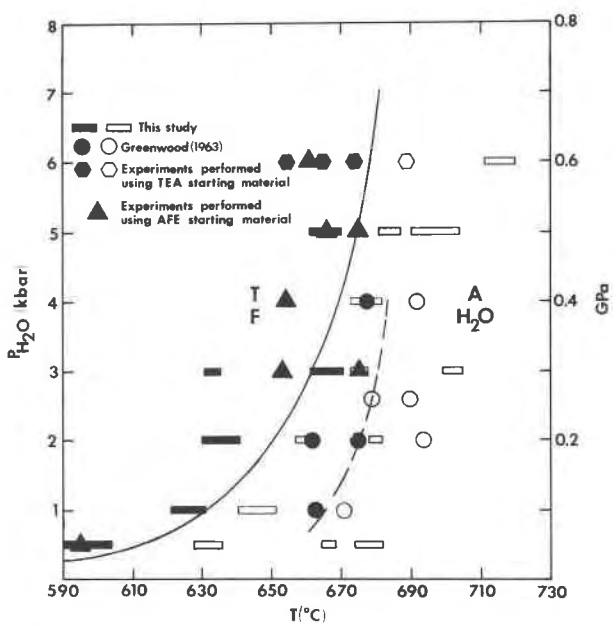

Fig. 6. Dehydration curve for the reaction 9T + 4F = 5A + 4H_2O. Solid symbols represent growth of the low temperature assemblage; open symbols represent growth of the high temperature assemblage. Size of rectangles represents uncertainty in the measurement of pressure and temperature. Dashed curve shows where Greenwood (1963) located this equilibrium.

enstatite and anthophyllite were almost entirely consumed in experiments TEA-23, -24 and -25 (Fig. 6, solid hexagons); if the assemblage T + F is stable under the conditions of these experiments, they probably lie on the low temperature side of TF = AW. In sharp contrast, forsterite was absent and anthophyllite grew in experiment TEA-19 (Fig. 6, open hexagon) suggesting that this experiment might lie on the high temperature side of the reaction TF = AW. Talc nucleated and grew in a number of experiments performed with the AFE starting material (Table 1). If the assemblage T + F + A is stable in these experiments, they probably lie on the low temperature side of TF = AW (Fig. 6). Although experiment AFE-20 lies on the high temperature side of the calculated curve, it does lie within the experimentally established bracket at $P_{H_2O} = 3$ kbar.

Our experimental data for this reaction are inconsistent with the data of Greenwood (1963). Our calculated curve which lies at the low temperature end of the 3 kbar experimental bracket is about 25°C lower than Greenwood's curve (Fig. 6). Perhaps the discrepancy is the result of differences in the starting material used to reverse the reaction. Greenwood used a starting material containing a fine-grained, intimate mixture of anthophyllite, clinoenstatite, cristobalite, talc and forsterite whereas the starting material used during this study did not contain clinoenstatite or cristobalite. Although Greenwood's starting material was far more reactive, as shown by higher degrees of conversion from one assemblage to another in experiments of shorter duration (compare Greenwood, 1963, Table 4 with this study, Table 1), it did contain extraneous phases; perhaps anthophyllite grew at the expense of the extraneous phases contained in Greenwood's starting material.

The reaction $A + F = 9E + H_2O$. Critical experiments bracketing the dehydration curve for the reaction AF = EW are listed in Table 1 and plotted on Figure 7. Talc spontaneously nucleated and grew in a number of experiments conducted on the low temperature side of AF = EW (Table 1). Talc growth in these experiments did not impair our ability to judge reaction direction. Due to the close spacing of the reactions emanating from the [Q] invariant point, growth of talc in some of the AF = EW experiments suggests that the experiments lie on the low temperature side of TF = AW as discussed previously. The nucleation and growth of anthophyllite in TF = EW experiments does not assist in locating AF = EW in P–T space because anthophyllite is stable on both sides of TF = EW. Although our experimental data for the reaction AF = EW are consistent with all of Greenwood's (1963) experiments (Fig. 7), our curve lies about 13°C lower than Greenwood's curve at $P_{H_2O} = 2$ kbar.

The reaction $T + 4E = A$. Critical experiments, the first reported in the literature, bracketing the equilibrium curve for the reaction TE = A are listed in Table 1 and plotted on Figure 8. Examination of Figure 1 indicates that anthophyllite is stable in the presence of excess H_2O along those segments of TE = A which lie between the [Q] and [F] invariant points and metastable in the presence of excess water along that portion of TE = A which lies between the

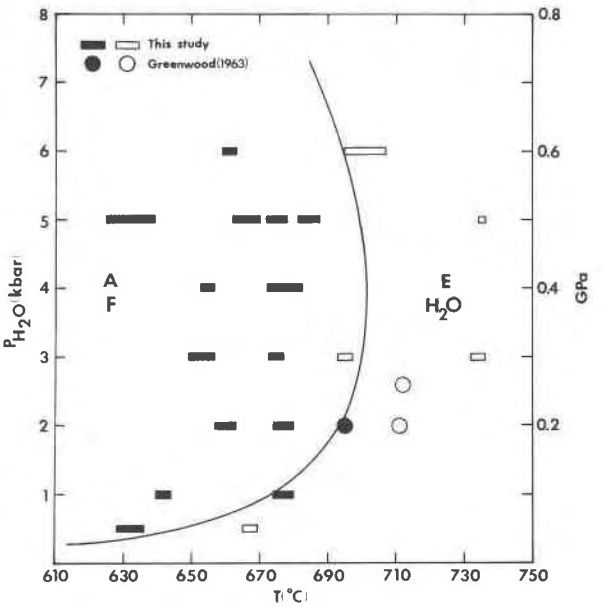

Fig. 7. Dehydration curve for the reaction A + F = 9E + H_2O. Solid symbols represent the growth of the low temperature assemblage; open symbols represent the growth of the high temperature assemblage. Size of rectangles represents uncertainty in the measurement of pressure and temperature.

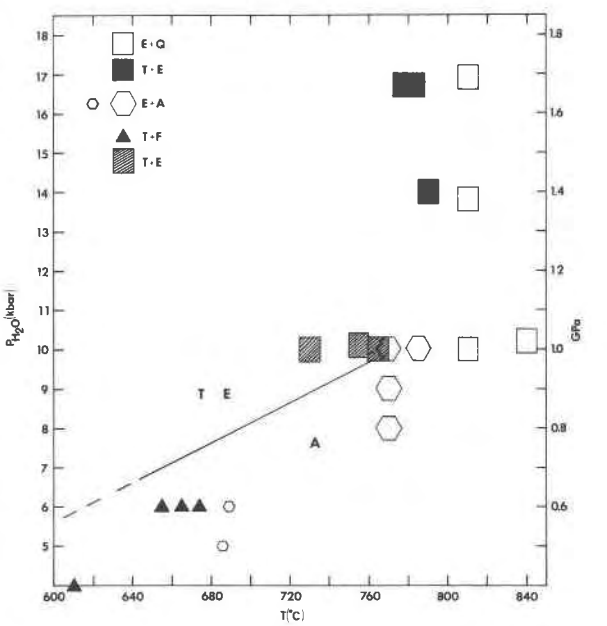

Fig. 8. Equilibrium curve for the solid–solid reaction T + 4E = A. Size of symbols represents approximate uncertainty in the measurement of pressure and temperature. The four experiments conducted above $P_{H_2O} = 13$ kbar clearly demonstrate that anthophyllite is unstable at high pressure and help define the location of the dehydration curve for the reaction T = EQW.

two [Q] invariant points. Although vapor-conservative, this reaction was reversed in the presence of excess water in order to promote reaction rate and to maintain hydrostatic pressure within the gold capsules containing the starting material.

Although somewhat ambiguous due to the nucleation and growth of new phases and the persistence of metastable phases, we believe that the experimental data for TE = A tightly constrain the position of this reaction at $P_{H_2O} = 10$ kbar and provide high temperature limits at 5 and 6 kbar.

Experiments performed with the TEA starting material at water pressures above 13 kbar clearly indicate that pure Mg anthophyllite is unstable at these pressures. Anthophyllite was completely decomposed in all four high-pressure experiments (Fig. 8). Talc and enstatite grew in the low-temperature pair of experiments (Fig. 8, large solid rectangles) whereas quartz nucleated and grew together with enstatite in the high temperature pair (large open rectangles). These experimental results suggest that T = EQW is a stable reaction at water pressures above 13 kbar. The high pressure experiments were used to help define the position of T = EQW (Fig. 2).

The seven experiments at $P_{H_2O} = 10$ kbar suggest that the [F] invariant point occurs at water pressures above 10 kbar. With increasing temperature the assemblage T + E (Fig. 8, partially filled rectangles) gives way to a relatively narrow field in which the assemblage A + E grows (Fig. 8, large hexagons), followed by a field in which the assemblage E + Q grows. The key to our interpretation is the narrow field containing A + E separating the T + E assemblage from the E + Q assemblage; examination of Figures 1 and 8 suggests that this can only occur if the invariant point lies at water pressures above 10 kbar. Because anthophyllite and enstatite both grew in the two experiments at 8 and 9 kbar (Fig. 8, large open hexagons), the equilibrium curve for TE = A must lie on the low temperature side (Fig. 8) of these experiments. Although the growth of T + E and E + Q from a starting material containing T, E and A and having a bulk composition corresponding to A is reasonable, growth of the assemblage A + E can only occur if the bulk composition of the starting material is either depleted in Si or enriched in Mg. Although quartz was not observed in the X-ray patterns, we suggest that some Si was dissolved in the vapor phase which constituted about 50 percent by weight of the charge. This suggestion is supported by the observation that Si was readily leached from experiments which developed a leak.

The experiments performed at and below water pressures of 6 kbar place high temperature limits on the position of the phase boundary for TE = A and help define the location of the [Q] invariant point. The four experiments designated by solid triangles in Figure 8 resulted in the growth of talc, the nucleation and growth of forsterite and the complete disappearance of anthophyllite and enstatite; in other words, the enstatite–H_2O and anthophyllite–H_2O tie lines were broken in favor of the talc–forsterite tie line. Enstatite and anthophyllite grew in the two experiments designated by small open hexagons (Fig. 8). If the [Q] invariant point were located at water pressures below 6 kbar, one would expect to encounter the assemblage T + E between the T + F and the E + A assemblages (Fig. 1). The assemblage T + E was not encountered at $P_{H_2O} = 6$ kbar suggesting that the [Q] invariant point lies at water pressures above 6 kbar. Because the assemblage T + F is stable on both sides of TE = A at water pressures below [Q], this assemblage cannot be used to place constraints on the position of TE = A. The phase boundary for TE = A must however lie on the low temperature side of the assemblage E + A at water pressures below [Q].

Discussion

A phase diagram for Mg-anthophyllite consistent with the phase equilibrium data set down in Table 2 and with the thermodynamic data discussed in Day et al. (1985) is shown in Figure 9. The diagram was constructed for the condition $P_{H_2O} = P_{Total}$; the effects of lowering the a_{H_2O} and of substituting "impurities" such as Fe in the Mg-silicates will be discussed later.

Although the experimentally determined brackets are tight, the high pressure [Q] and [F] invariant points are difficult to locate precisely because the curves are closely-spaced and intersect at shallow angles. However, as dis-

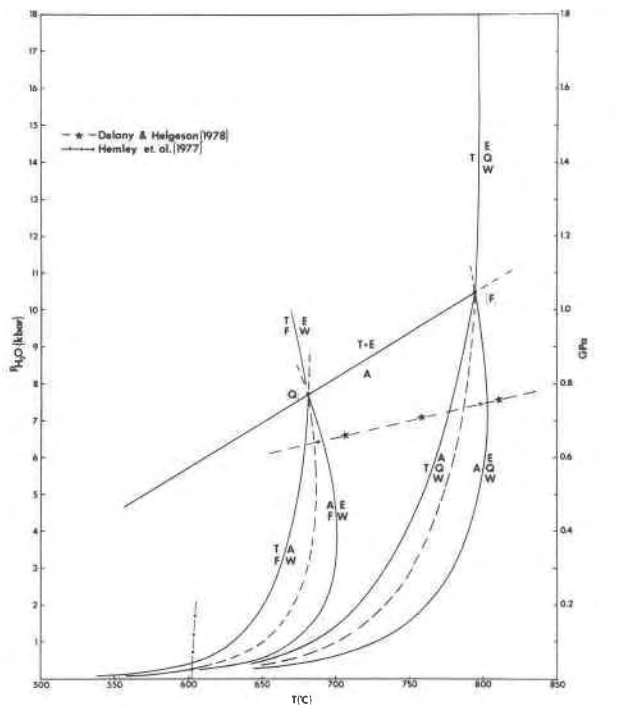

Fig. 9. Phase diagram for anthophyllite consistent with the phase equilibrium data presented in Table 1 and in Figs. 2 through 8, and consistent with the molar volumes and heat capacities of the minerals involved in the equilibria of interest. Equilibrium curves for the reaction TE = A calculated by Hemley et al. (1977) and Delany and Helgeson (1978) are included for comparison.

cussed in our companion paper (Day et al., 1985), thermodynamically consistent invariant points lie at 10.5 ± 1.0 kbar, 794 ± 10°C for [F] and 7.7 ± 0.5 kbar, 682 ± 10°C for [Q]. The low-pressure [Q] and [F] invariant points are also difficult to locate but appear to occur at water pressures below 100 bars and temperatures below 400°C and may be metastable with respect to serpentine-bearing equilibria.

The phase diagram depicted on Figure 9 differs considerably from the diagram first proposed by Greenwood (1963) and later modified by him (Greenwood, 1971) and from the diagram proposed by Hemley et al. (1977) even though the experimental data upon which all of these diagrams are based are, for the most part, in excellent agreement. The chief reason for the discrepancy is that the available thermodynamic data are not sufficiently precise to allow extrapolation of the equilibria far outside the pressure range in which the bracketing experiments were performed. In addition, until now, experimental data for the reaction TE = A were unavailable. Because TE = A does not involve a volatile phase, ΔS and ΔV of reaction are small hence the position of this reaction in P–T space is very sensitive to small changes in the thermodynamic properties of the constituent phases. For example, the phase boundary for TE = A calculated by Greenwood (1971) lies more than 200°C below the position calculated by Hemley et al. (1977) at $P_{H_2O} = 2$ kbar (Fig. 9). Although Delany and Helgeson (1978) used Hemley et al.'s (1977) solubility data, which were obtained at $P_{H_2O} = 1$ kbar, to calculate a phase diagram for Mg-anthophyllite, their diagram differs markedly from the one proposed by Hemley et al. (1977) who suggested that the low pressure [Q] and [F] invariant points are stable and that the corresponding high pressure invariant points are metastable; the opposite viewpoint was supported by Delany and Helgeson (1978). Although Delany and Helgeson's calculated slope for TE = A is slightly flatter than ours (Fig. 9), the topology and calculated positions for the relevant equilibria are in remarkably good agreement with our diagram especially when uncertainties involved in calculating equilibrium curves are considered.

Application to rocks

Although the presence of additional components, notably FeO and CO_2, may substantially influence the positions of the curves, the phase relations for Mg-anthophyllite depicted on Figure 9 are in general accord with field observations. The assemblage T + F which is limited by the reactions TF = AW and An = FTW has a stability field about 140°C wide which is in good agreement with the field-based estimate of Evans (1977). The assemblage A + F which is limited by the reactions TF = AW and AF = EW has a stability field about 50°C wide for water pressures of 2 to 3 kbar; the stability field for A + F narrows with increasing pressure and is terminated by the [Q] invariant point at about $P_{H_2O} = 7.5$ kbar.

Evans and Trommsdorff (1974) observed that enstatite and talc coexist in textural equilibrium in rocks recrystallized at 600 ± 100°C and P_{H_2O} about 7 kbar. Although these observations are consistent with the phase diagram presented in Figure 9, the minerals involved contain iron which markedly affects the position of the reaction TE = A.

Rabbitt (1948) and Sanford (1977) observed the "stable" coexistence of An + A + T. Hemley et al. (1977) and Sanford (1977) postulated that the reactions An = FTW and TF = AW intersect and generate an invariant point (Fig. 10) involving the phases A, An, F, T and W. According to Hemley et al. (1977, p. 369), the invariant point occurs at water pressures above 10 kbar with the assemblage An + A + T stable on the high pressure side of the invariant point; in other words, these authors believe that the enantiomorphic form of the topology shown on Figure 10 is correct. On the other hand, Sanford suggested that the orientation shown in Figure 10 with the assemblage An + A + T on the low pressure side of the invariant point is correct. The phase equilibrium data reported in this paper and the thermodynamic analysis by Day et al. (1985) suggest that a stable invariant point does not exist at high pressure. Although our phase diagram is consistent with the orientation proposed by Sanford, the calculations (Day et al., 1985) suggest that if the invariant point occurs at low pressure, it must lie at a water pressure less than 100 bars and a temperature less than 350°C. In either case, our analysis suggests that in Fe-free rocks, An + A + T is not likely to be observed as a stable assemblage.

Influence of other components on anthophyllite phase relations

Although the Mg-anthophyllites found in metamorphosed siliceous dolomites are relatively pure, the fluid phase coexisting with these anthophyllites probably contained a significant CO_2 content. Anthophyllites from ultramafic rocks commonly contain about 10 mole percent

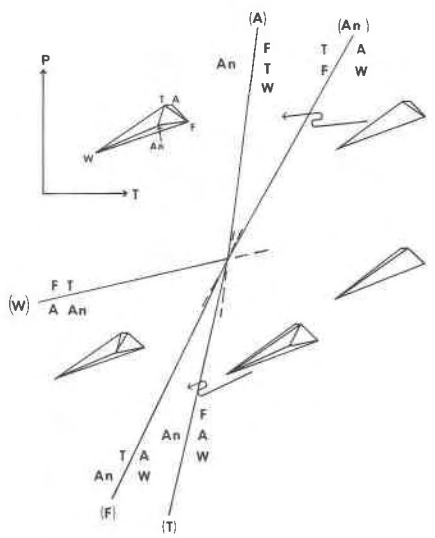

Fig. 10. Invariant point at which anthophyllite, antigorite, forsterite, talc and water are in equilibrium.

FeO and often coexist with fluids containing CO_2. Hence it is important to consider the effect of additional components on the phase relations depicted on Figure 9.

Decreasing the a_{H_2O} in the fluid phase will cause dehydration reactions to be displaced toward lower temperatures but will not effect vapor conservative reactions such as TE = A (Greenwood, 1961). As the dehydration reactions are displaced with respect to TE = A, the [Q] and [F] invariant points will progressively "slide" down the curve for TE = A toward lower pressures and temperatures with decreasing a_{H_2O}. Although the stability field for the assemblage A + F will be restricted to lower pressures, it will widen because the reaction TF = AW which involves four moles of H_2O will be displaced further toward lower temperatures than AF = EW which involves only one mole of H_2O.

Evans (1977) evaluated the effect of substituting Fe for Mg on the positions of the equilibria shown on Figure 9. When average Mg/(Mg + Fe) ratios for the appropriate minerals are used, the displacement of the dehydration reactions under consideration range from +10°C for AF = EW to −40°C for TF = AW. Since the width of the A + F stability field is governed by the reactions AF = EW and TF = AW, the substitution of appropriate amounts of Fe in the Mg-silicates will increase the width of this field (Evans, 1977) from 50°C in the Fe-free system to about 100°C in the Fe-bearing system. Evans and Trommsdorff (1974) calculated that the reaction TE = A would be displaced by about −180°C due to the substitution of realistic amounts of Fe in the Mg-silicates. Hence the locations of invariant points [Q] and [F] depend on the Mg/(Mg + Fe) ratios of the minerals stable at each invariant point. A decrease in Mg/(Mg + Fe) results in a shift of [Q] and [F] toward higher pressures and somewhat lower temperatures.

In an attempt to explain the occurrence of the assemblage An + A + T, Sanford (1977) calculated (at 2 and 6 kbar and at $a_{H_2O} = 1$) that the substitution of appropriate amounts Fe for Mg would lower TF = AW by −120 to −150°C rather than by −37°C as calculated by Trommsdorff and Evans (1974) and would raise the invariant point depicted on Figure 10 to a pressure regime which might be attained in nature. Unfortunately, the details of Sanford's calculations were not provided in his abstract. It should be pointed out that all such calculations are heavily dependent on the ΔS assumed for the reaction.

Acknowledgments

Discussions with H. J. Greenwood and E-an Zen throughout JVC's involvement with anthophyllite phase relations have been both stimulating and fruitful. T. J. B. Holland kindly provided some unpublished experimental data. R. C. Newton is especially thanked for generously providing the laboratory facilities and supplies (funded by NSF Grant EAR 78-15939 to R. C. Newton) which enabled JVC to perform the high pressure experiments discussed in this paper. R. C. Newton, D. M. Jenkins and D. Perkins III provided invaluable advice and assistance in carrying out the high pressure experiments. Discussions with G. R. Robinson concerning the thermodynamic parameters for the minerals of interest were very helpful. Perceptive reviews by R. G. Berman, T. J. B. Holland and M. Engi resulted in substantial improvements in the manuscript. Financial support throughout the study was provided by NSF Grants EAR 74-13393 AOI and EAR-7904092 to JVC and EAR77-22775 to HWD.

References

Appleman, D. E. and Evans, H. T., Jr. (1973) Job 9214: Indexing and least squares refinement of powder diffraction data. National Technical Information Service, U.S. Department of Commerce, Springfield, Virginia, Document PB-216 188.

Bowen, N. L. and Tuttle, O. F. (1949) The system MgO–SiO_2–H_2O. Geological Society of America Bulletin, 60, 439–460.

Chernosky, J. V., Jr. (1973) An experimental investigation of the serpentine and chlorite group minerals in the system MgO–Al_2O_3–SiO_2–H_2O. Ph.D. Thesis, Massachusetts Institute of Technology, Cambridge, Massachusetts.

Chernosky, J. V., Jr. (1976) The stability field of anthophyllite—A reevaluation based on new experimental data. American Mineralogist, 61, 1145–1155.

Chernosky, J. V., Jr. and Autio, L. K. (1979) The stability of anthophyllite in the presence of quartz. American Mineralogist, 64, 294–303.

Chernosky, J. V., Jr., Day, H. W. and Caruso, L. J. (1982) A phase diagram for Mg-anthophyllite (abstr.). Transactions of the American Geophysical Union, 63, 1151.

Danckwerth, P. A. and Newton, R. C. (1978). Experimental determination of the spinel peridotite to garnet peridotite reaction in the system MgO–Al_2O_3–SiO_2 in the range 900–1100°C and Al_2O_3 isopleths of enstatite in the spinel field. Contributions to Mineralogy and Petrology, 66, 189–201.

Day, H. W. and Halbach, H. (1979) The stability field of anthophyllite: The effect of experimental uncertainty on permissible phase diagram topologies. American Mineralogist, 64, 809–823.

Day, H. W., Chernosky, J. V. and Kumin, H. J. (1985) Equilibria in the system MgO–SiO_2–H_2O: A thermodynamic analysis. American Mineralogist, 70, 237–248.

Delany, J. M. and Helgeson, H. C. (1978) Calculation of the thermodynamic consequences of dehydration in subducting oceanic crust to 100 Kb and >800°C. American Journal of Science, 278, 638–686.

Evans, B. W. (1977) Metamorphism of Alpine peridotite and serpentinite. Annual Reviews Earth and Planetary Sciences, 5, 397–447.

Evans, B. W. and Trommsdorff, V. (1974) Stability of enstatite + talc, and CO_2-metasomatism of metaperidotite, Val d'Efra, Lepontine Alps. American Journal of Science, 274, 274–296.

Fisher, G. W. and Medaris, L. C., Jr. (1969) Cell dimensions and X-ray determinative curve for synthetic Mg–Fe olivines. American Mineralogist, 54, 741–753.

Forbes, W. C. (1971) Iron content of talc in the system $Mg_3Si_4O_{10}(OH)_2$–$Fe_3Si_4O_{10}(OH)_2$. Journal of Geology, 79, 63–74.

Fyfe, W. S. (1962) On the relative stabilities of talc, anthophyllite and enstatite. American Journal of Science, 270, 151–154.

Greenwood, H. J. (1961) The system $NaAlSi_2O_6$–H_2O–Argon: Total pressure and water pressure in metamorphism. Journal of Geophysical Research, 66, 3923–3946.

Greenwood, H. J. (1963) The synthesis and stability field of anthophyllite. Journal of Petrology, 4, 317–351.

Greenwood, H. J. (1971) Anthophyllite. Corrections and com-

ments on its stability. American Journal of Science, 270, 151–154.

Helgeson, H. C., Delany, J. M., Nesbitt, H. W., and Bird, D. K. (1978) Summary and critique of the thermodynamic properties of rock-forming minerals. American Journal of Science, 278-A, 1–219.

Hemley, J. J., Montoya, J. W., Shaw, D. R., and Luce, R. W. (1977) Mineral equilibria in the $MgO–SiO_2–H_2O$ system: II Talc–antigorite–forsterite–anthophyllite–enstatite stability relations and some geologic implications in the system. American Journal of Science, 277, 353–383.

Johannes, W. (1973) A simplified piston-cylinder apparatus of high precision. Neues Jahrbuch für Mineralogie-Monatshefte, 337.

Johannes, W. (1975) Zur Synthese and thermischen Stabilitat von Antigorit. Forschritte der Mineralogie, 53, 1–36.

Kitahara, S., Takenouchi, S., and Kennedy, G. C. (1966) Phase relations in the system $MgO–SiO_2–H_2O$ at high temperatures and pressures. American Journal of Science, 264, 223–233.

Rabbitt, J. V. (1948) A new study of the anthophyllite series. American Mineralogist, 33, 263–323.

Robie, R. A., Bethke, P. M., and Beardsley, K. M. (1967) Selected X-ray crystallographic data, molar volumes, and densities of minerals and related substances. United States Geological Survey Bulletin 1248.

Robie, R. A., Hemingway, B. S., and Fisher, J. R. (1978) Thermodynamic properties of minerals and related substances at 298.15 K and 1 bar (10^5 Pascals) pressure and at higher temperatures. United States Geological Survey Bulletin 1452.

Sanford, R. F. (1977) The coexistence of antigorite and anthophyllite in ultramafic rocks. (abstr.) Geological Society of America Abstracts with Programs, 9, 1154–1155.

Skippen, G. B. (1971) Experimental data for reactions in siliceous marbles. Journal of Geology, 79, 457–481.

Trommsdorff, V. and Evans, B. W. (1974) Alpine metamorphism of peridotitic rocks. Schweizerische Mineralogische und Petrographische Mitteilungen, 54, 333–352.

Usdansky, S. I., Mohr, R. E., and Stout, J. H. (1978) Some topological constraints on the stability of anthophyllite. (abstr.) Geological Society of America Abstracts with Programs, 10, 507–508.

Weeks, W. A. (1956) Heats of formation of metamorphic minerals in the system $CaO–MgO–SiO_2–H_2O$ and their petrological significance. Journal of Geology, 64, 456–472.

Zen, E-an (1977) The phase-equilibrium calorimeter, the petrogenetic grid, and a tyranny of numbers. American Mineralogist, 62, 189–204.

Manuscript received, December 1, 1983;
accepted for publication, October 12, 1984.